POLYPUBLIE

Enhancing the optical performance of oxyfluoride glass ceramics by optimizing the oxide: Fluoride ratio and crystallinity for optical refrigeration

Jyothis Thomas, Thomas Meyneng, Yannick Ledemi, Anthony Roberge, Frederic Monet, Denis Seletskiy, Younès Messaddeq, Raman Kashyap

Document en libre accès dans PolyPublie
Open Access document in PolyPublie

Date	2023
Type	Article de revue / Article
Version	
URL de PolyPublie PolyPublie URL	https://publications.polymtl.ca/54795/
Évaluation par les pairs Peer reviewed	Révisé par les pairs / Refereed
Conditions d'utilisation Terms of use	Creative Commons Attribution-Utilisation non commerciale-Pas d'oeuvre dérivée 4.0 International / Creative Commons Attribution-NonCommercial-NoDerivatives 4.0 International (CC BY-NC-ND)
Référence Citation	Thomas, J., Meyneng, T., Ledemi, Y., Roberge, A., Monet, F., Seletskiy, D., Messaddeq, Y., & Kashyap, R. (2023). Enhancing the optical performance of oxyfluoride glass ceramics by optimizing the oxide: Fluoride ratio and crystallinity for optical refrigeration. Journal of Non-Crystalline Solids: X, 17, 10 pages. https://doi.org/10.1016/j.nocx.2023.100173

Publication officielle
Official publication

Titre de la revue Journal title	Journal of Non-Crystalline Solids: X (vol. 17)
Maison d'édition Publisher	Elsevier B.V.
URL officielle Official URL	https://doi.org/10.1016/j.nocx.2023.100173
Mention légale Legal notice	© 2023 The Author(s). Published by Elsevier B.V. This is an open access article under the CC BY-NC-ND license (http://creativecommons.org/licenses/bync-nd/4.0/).

Ce fichier a été téléchargé à partir de PolyPublie, le dépôt institutionnel de Polytechnique Montréal
This file has been downloaded from PolyPublie, the institutional repository of Polytechnique Montréal
https://publications.polymtl.ca

Journal of Non-Crystalline Solids: X 17 (2023) 100173

Contents lists available at ScienceDirect

Journal of Non-Crystalline Solids: X

journal homepage: www.sciencedirect.com/journal/journal-of-non-crystalline-solids-x

Enhancing the optical performance of oxyfluoride glass ceramics by optimizing the oxide: Fluoride ratio and crystallinity for optical refrigeration

Jyothis Thomas [a,*], Thomas Meyneng [b], Yannick Ledemi [b], Anthony Roberge [a], Frederic Monet [a], Denis Seletskiy [c], Younès Messaddeq [b], Raman Kashyap [a,d]

[a] Fabulas Laboratory, Department of Engineering Physics, École Polytechnique de Montréal, P.O. Box 6079, Station Centre-ville, Montréal, QC H3C 3A7, Canada
[b] Centre d'Optique, Photonique et Laser, 2375 Rue de la Terrasse, Université Laval, Québec, QC G1V 0A6, Canada
[c] femtoQ Laboratory, Department of Engineering Physics, Polytechnique Montreal, 2900 Blvd Edouard-Montpetit, Montreal H3T 1J4, Canada
[d] Fabulas Laboratory, Department of Electrical Engineering, École Polytechnique de Montréal, P.O. Box 6079, Station Centre-ville, Montréal, QC H3C 3A7, Canada

ARTICLE INFO

Keywords:
Oxyfluoride glass ceramics
Photoluminescence quantum yield
Laser cooling

ABSTRACT

The optimization of the oxide and fluoride content, crystallinity and rare earth ion concentration in oxyfluoride glass ceramics (GCs) are of great importance in obtaining high photoluminescence quantum yield (PLQY) for optical refrigeration applications. Presented herein are the important advancements in the development of a novel oxyfluoride GCS of the composition $(SiO_2\text{-}Al_2O_3)_{(100\text{-}a)}$ $(YLiF_4)_b$: $(YbF_3)_b$ (a = 35 and 40; in mol %, b = 1 and 2 mol%) with the corresponding parent glasses with an in-depth investigation on enhancing the optical performance for laser cooling. Depending on the oxide/fluoride (O/F) ratio and ytterbium content the internal quantum yield (iQY) varied between 70 and 99% in glass ceramics at several excitation wavelengths. The optical properties of GCs containing $YLiF_4$ and YF_3 nanocrystals obtained from the same initial composition (modulated by time and fusion temperature) were compared to find the optimal composition for optical refrigeration. Low fluorine content led to the generation of $YLiF_4$ as a major phase after ceramization and high fluorine content helped in the generation of the YF_3 phase. An increase in the radiative lifetime of YF_3 GCs compared to $YLiF_4$ GCs has been found to coincide with the enhancement of the PLQY, which is beneficial for laser cooling. The temperature change (ΔT) change measured using a fiber Bragg grating (FBG) in the glass and glass-ceramic samples with different pump wavelengths showed significant heat mitigation near ~1030 nm. The observed enhanced PL intensity, iQY and lifetime after purification of $YLiF_4$ glasses imply that the purity of the material plays a paramount role in lowering the background absorption and enhancing the quantum yield. Looking ahead, we see a bright future for oxyfluoride GCs in applications requiring the ultimate levels of thermal, mechanical and optical performance, especially for the development of cryocooler devices, which are still technologically challenging and expensive. The usage of GCs will open up new possibilities in optical cooling technology, enabling cooling devices of any size and shape.

1. Introduction

Solid-state laser cooling has emerged as an exciting research area recently driven by the rapidly increasing demand for cryocooler devices, sensors and satellite instruments, radiation balanced lasers etc. requiring low mechanical vibrations, no mechanical components and enhanced reliability [1,2]. To meet the requirements of the aforementioned applications, new innovative materials with higher quantum efficiency and low background absorption is of great significance. Although the solid-state laser cooling technique was proposed more than a century ago [3], the enormous interest in optical properties of crystals and glass ceramics had arisen only after 65 years with the observation of laser cooling in ZBLAN glasses [4], thanks to the advances in purification required for the fabrication of high quality optical fibers. Lately, many materials with unprecedented properties have been proposed and studied [5–9]. Among them, the oxyfluoride glass ceramics (GCs) represent a class of promising materials due to their specific advantages relative to crystals and a range of other unique and important properties.

* Corresponding author.
E-mail address: jyothis.thomas@polymtl.ca (J. Thomas).

https://doi.org/10.1016/j.nocx.2023.100173
Received 18 December 2022; Received in revised form 12 February 2023; Accepted 16 February 2023
Available online 20 February 2023
2590-1591/© 2023 The Author(s). Published by Elsevier B.V. This is an open access article under the CC BY-NC-ND license (http://creativecommons.org/licenses/by-nc-nd/4.0/).

Many ground-breaking experiments have already shown the great potential of glasses for laser cooling [10–12]. Furthermore, GCs offer advantages compared to crystals and semiconductors, they enable the control of the shape and size, which can be explored for producing optical fibers. Higher optical transparency, thermomechanical strength and easy moulding make glass a preferred photonic platform material [13–17].

In the past decade, oxyfluoride glass ceramics with different hosts consisting of nano-crystals of PbF_2, LaF_3, BaF_2, $BaYF_5$, $NaYF_4$, etc. with interesting optical properties have become of great interest [18–20]. In recent years, the development and applications in solid state laser cooling have been widely explored by our group owing to its near unity quantum yield and the excellent mechanical and thermal stability [21–30]. The transparent GC is fabricated by applying thermal treatment to the parent glass [18]. The multi phonon decay as well as non-radiative transition probability in such materials are lower since RE ions are predominantly distributed in low phonon energy nanocrystals making it a promising material for laser cooling [23]. For efficient cooling it is of great importance to choose the RE ion and host matrix that offers a near-unity quantum efficiency along with higher purity. Therefore, in the current work, we explored GCs containing $YLiF_4$ and YF_3 nanocrystals and studied the structural and optical properties of those glasses with different compositional variations. The RE- doped glass ceramics containing $YLiF_4$ nanocrystals have been studied by several groups for display devices, lasers and other opto-electronic applications [22,31,32]. But a detailed study of their optical properties is absent in the literature and those glasses have not yet been explored for laser cooling. Recently $YLiF_4$ nanocrystals embedded transparent glass–ceramics were fabricated by controlled heat-treatments of LiF-YF_3-Al_2O_3-SiO_2 glass by Suzuki et al [28]. Their studies were focused on incorporating RE ions such as Er^{3+} and Eu^{3+} into $YLiF_4$ nanocrystals in the glass–ceramics. It is already known that $YLiF_4$ crystals are ideal matrices for trivalent Yb ions which can substitute the Y^{3+} ions as a dopant [33,34]. Similarly, YF_3 crystals also possess a low phonon energy ($\sim$358 cm^{-1}) and the Y^{3+} ion sites can be easily replaced by trivalent Yb^{3+} ions. Therefore, it is highly desirable to utilize them as an optical cooling material.

A highly purified glass is the most demanding challenge in demonstrating cooling in GCs [23,25]. Owing to the undesirable impurities and other detrimental components, it is challenging to achieve lower background absorption. This has led to enormous attempts around the world for the synthesis of highly pure glass by various processes and purification techniques [35,36]. Nevertheless, using limited handful facilities, obtaining near unity quantum yield and minimizing background absorption which are essential for optical refrigeration, remain as significant challenges. Along with the purity, optimizing the oxide: fluoride content in oxyfluoride glass ceramics is paramount to maximizing the quantum yield that will ultimately set the optical performance limits of GC for optical cooling.

In this work, we experimentally separate or unveil four mechanisms that contribute to the PL enhancement and govern the PL emission properties (quantum yield, lifetime etc.) and cooling characteristics of oxyfluoride glass ceramic namely, (i) the oxide: fluoride ratio, (ii) ytterbium ion concentration, (iii) amount of crystallinity and (iv) the purity of the material. First, we address the impact of the O/F ratio on GCs and corresponding parent glasses by comparing different samples (See Table 1). In the quantum yield and lifetime measurements we note a strong dependence of the emission properties on the O/F ratio and thus the cooling characteristics. Second, we address the impact of ytterbium ion concentration (in mol %) as we compare the PL emission from samples doped with 1 mol% to 2 mol% of ytterbium. The GC doped with 2 mol% was found to be most suitable for cooling applications. Thirdly, the optical properties of GCs containing YF_3 nano crystals and $YLiF_4$ crystals obtained from the same initial composition (modulated by time and temperature of the fusion) were compared to find the optimal composition for optical refrigeration. GCs with YF_3 crystals having a higher fluorine concentration and higher crystalline fraction benefiting from the low phonon energy were found to be most suitable for laser cooling compared with the one having a low fluorine concentration and lower crystalline fraction. Finally, we compared the optical properties of purified GCs with that of not purified GCs and found that the purification helps to enhance the PL emission intensity and iQY along with lowering the background absorption.

Table 1
The glass ceramic and parent glass compositions along with the terminology used in the text.

Glass-ceramics composition	Terminology	Parent Glass composition	Terminology
$(SiO_2\text{-}Al_2O_3)_{65}$-$(YLiF_4)_{35}$: $(YbF_3)_1$	GC 65:35:1	$(SiO_2\text{-}Al_2O_3)_{65}$-$(YLiF_4)_{35}$: $(YbF_3)_1$	G 65:35:1
$(SiO_2\text{-}Al_2O_3)_{60}$-$(YLiF_4)_{40}$: $(YbF_3)_1$	GC 60:40:1	$(SiO_2\text{-}Al_2O_3)_{60}$-$(YLiF_4)_{40}$: $(YbF_3)_1$	G 60:40:1
$(SiO_2\text{-}Al_2O_3)_{65}$-$(YLiF_4)_{35}$: $(YbF_3)_2$	GC 65:35:2	$(SiO_2\text{-}Al_2O_3)_{65}$-$(YLiF_4)_{35}$: $(YbF_3)_2$	G 65:35:2
$(SiO_2\text{-}Al_2O_3)_{60}$-$(YLiF_4)_{40}$: $(YbF_3)_2$	GC 60:40:2	$(SiO_2\text{-}Al_2O_3)_{60}$-$(YLiF_4)_{40}$: $(YbF_3)_2$	G 60:40:2
$(SiO_2\text{-}Al_2O_3)_{60}$-$(YF_3)_{40}$: $(YbF_3)_2$	YF_3GC 60:40:2	$(SiO_2\text{-}Al_2O_3)_{60}$-$(YF_3)_{40}$: $(YbF_3)_2$	YF_3G 60:40:2

2. Materials and methods

2.1. Sample preparation and characterization

The selected Gs and GCs pertinent to the following chemical composition in mol %: $(SiO_2\text{-}Al_2O_3)_{(100\text{-}a)}$ $(YLiF_4)_b$: $(YbF_3)_b$ (a = 35 and 40; in mol %, b = 1 and 2; in mol %) were made by the conventional melt quenching technique. Calculated amounts of precursor materials were mixed in an agate mortar in a glove box in a dry nitrogen atmosphere, and thereafter heated up to the melting temperature of 1530°C in a platinum crucible for 10 min. Afterward, the melt was poured into a preheated brass mold at 520°C followed by annealing at the glass-transition temperature for 2 h, to relieve cooling stresses. GCs containing YF_3 crystals were prepared at a fusion temperature of 1430 °C for 10 min inside of a platinum DPH (expand) crucible, under a dry argon atmosphere. The melt was then cast in a stainless steel mold that had been preheated to 520 °C, and annealed for two hours [37]. The GCs containing $YLiF_4$ nanocrystals were fabricated by using a heat treatment using 600 °C for 4 h. Ceramization of GCs containing YF_3 phase was performed at 580 °C for 4 h in a Nabertherm L-092S3RN3 under ambient air atmosphere.

A differential scanning calorimeter (Netzsch DSC, 404 F3 Pegasus) equipped with a liquid nitrogen cooling unit and a type S thermocouple sensor was used to measure the glass transition (T_g) and onset of crystallization (T_x) temperatures of both glass samples, at a heating rate of 10 °C/min in platinum pans up to 1000°C under inert atmospheric conditions. To determine accurately their heat capacity at room temperature, the same apparatus was employed using helium as flowing gas, a more sensitive type E thermocouple sensor, a heating rate of 4° C /min from −50°C to 100° C, uncovered aluminium sample pans and reference materials (sapphire).

The elemental analysis wes performed using inductively coupled plasma mass spectrometry (ICP-MS) on an Agilent 8800 – ICP MS. 100 mg of samples were digested in lightly heated nitric acid. Concentration of iron (Fe) was measured with the calibration of 10 standards from 0.1 ppb to 500 ppb.

2.2. Optical measurements

Ultraviolet - visible - near infrared (UV–Vis-NIR) transmission spectra (resolution of 2.0 nm) of the samples (~2.0 mm-thick) were measured using an Agilent Cary 5000 double-beam spectrophotometer.

An M prism coupler (Metricon 2010) was used to measure the linear refractive index (RI) of the samples.

The photoluminescence (PL) emission spectra and quantum yield (QY) of the samples were measured using a Ti: Sapphire laser (Spectra-Physics 3900S) at pump wavelengths of 920 nm, 980 nm, and 1020 nm. An integrating sphere (Thorlabs IS200–4) connected to a multimode optical fiber to an Ando AQ6317B optical spectrum analyzer (OSA) was used to collect the emitted light.

The PL lifetime (τ) values ascribed to the Yb^{3+}: $2F_{5/2}$ level were obtained using a fast oscilloscope (Tektronix). A Thorlabs SM05PD1B photodiode along with a benchtop trans impedance amplifier was used to record the signal. To modulate the external signal, a Thorlabs MC100A chopper (frequency of 20.0 Hz) was employed. The pump wavelength was eliminated using an edge filter.

The steady-state temperature change of glasses and glass ceramics were measured while exciting with different pump wavelengths (980–1040 nm) from a the Ti: sapphire laser. Fig. 1 shows a schematic representation of the experiment.

The samples were placed on a couple of silica optical fibers that were mounted on a stainless-steel holder, to reduce the heat load on the glasses. A fiber Bragg grating (FBG) contact method [38] was used for temperature measurements. A broadband source and an optical circulator with the second port connected to the grating were employed for calibration. The reflection from the FBG is collected through the circulator's third port, where it is analyzed by an optical spectrum analyzer (Ando AQ6317B). A combination of half-wave plate (HWP) and Glan-Thompson polarizer (GLTp) was used to adjust the laser output power.

The background absorption coefficient (α_b) was determined using calorimetric technique while exciting the samples with 3 W at 1550 nm from an IPG ELR-70-1550-LP ytterbium-erbium fiber [23,25].

3. Results and discussion

For our study, we chose aluminosilicate oxyfluoride glass as a host matrix for several reasons: First, the embedded nanocrystals enable the full exploitation of the PL properties towards various optoelectronic applications. Moreover, the presence of low phonon energy nanocrystals ($YLiF_4$ and YF_3) within the glass matrix can be exploited towards enhancing and manipulating the PL properties of GC and thus the cooling characteristics. Finally, the silicate glass has a glass transition temperature of ~550°C, which is enough for fiber production. The compositions of investigated glasses and glass ceramics are listed in Table 1. In the terminology used to describe the samples, the first number represents the fluoride ratio followed by the oxide ratio and ytterbium ion concentration.

A very interesting feature of this composition is the fluorine concentration of the final glass which was modulated by the time and fusion temperature [37]. A lower fluorine content led to the generation of $YLiF_4$ as a major phase after ceramization, on the other hand, a higher fluorine content led to the generation of YF_3.

3.1. The thermal stability

The glass transition temperature Tg, onset crystallization temperature Tx, and the peak crystallization temperature (Tp) determined by DSC for GC 65:35:1 and GC 60:40:1 is depicted in Fig. 2(a-b). T_g was obtained from the inflection point on the enthalpy curve. For the parent glasses used to prepare the GC 65:35:1 and GC 65:35:2 samples, the glass transition temperature Tg was 581°C. For GC 60:40:1 and GC 60:40:2 it was 569°C. The onset crystallization temperature Tx was 765° C and 758° C, respectively. The Hruby parameter ($\Delta T = Tx - Tg$) was used to determine the glass thermal stability vs crystallization. The parent glass of composition $(SiO_2\text{-}Al_2O_3)_{65}\text{-}(YLiF_4)_{35}$: $(YbF_3)_1$ has a ΔT value of 184. For $(SiO_2\text{-}Al_2O_3)_{60}\text{-}(YLiF_4)_{40}$: $(YbF_3)_1$, it was 189°C. The high stability of both the glass shows their potential for shaping and fiber production. The glass transition temperature Tg, onset crystallization temperature Tx and the peak crystallization temperature (Tp) evaluated by DSC for YF_3GC 60:40:2 was 531°C, 670°C, and 695°C (Fig. 2(c)).

The thermal properties of glasses were significantly influenced by the fluoride content. The specific heat capacity (Cp) at 300 K for sample GC 65:35:1 was 0.73 J/K/Kg. The increase of fluorine ratio in sample G 60:40:1 resulted in a decrease of the Tg and a decrease of specific heat (0.68 J/K/Kg) accompanying the glass transition region. Since fluorine is a powerful network disrupter, it replaces the oxygen ions from the glass matrix and thus increases the chance for $YLiF_4$ crystallization in the glass [39]. Also due to the shifting of the initial ceramization temperature to lower temperatures, the stability against the crystallization parameter ($\Delta T = Tx - Tg$) is increased. In short, all the investigated glasses exhibit good thermal stability which is good for fiber production. Our findings are in good agreement with the previous works on aluminosilicate, and silicate-based glasses which contain fluorine [40,41].

3.2. Optical transmission and refractive index properties

Optical transparency is one of the most important properties of GCs used for optical cooling. The near IR transmission spectra of the prepared Gs and GCs are shown in Fig. 3(a-d). As observed in Fig. 3(a), for GC 65:35:2, the transparency was ~75% and 85% in the visible and NIR region respectively. But the corresponding glass (G 65:35:2) presented a higher transparency of ~82% and ~ 92% in the visible and NIR region

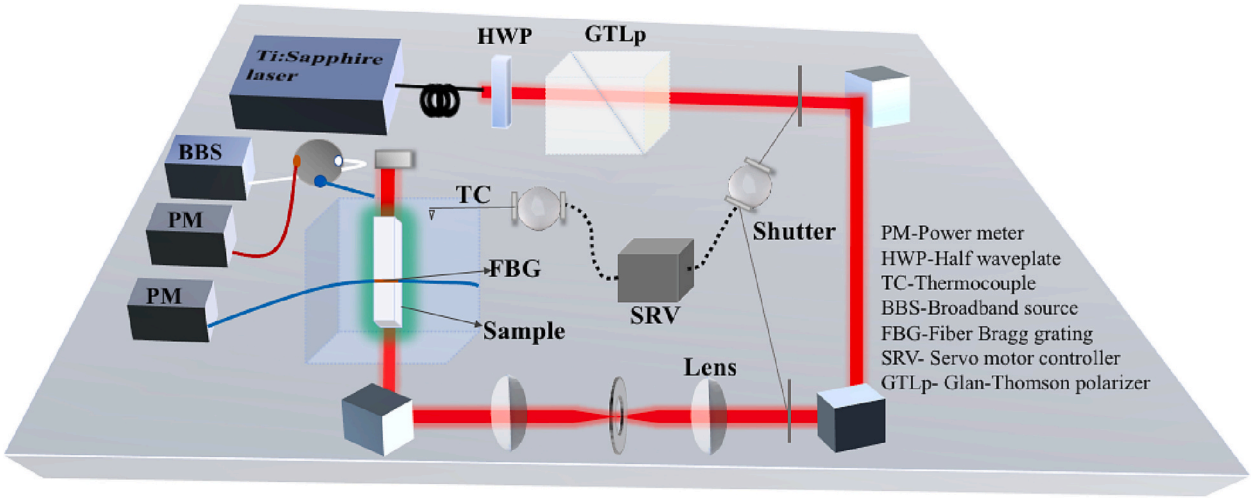


Fig. 1. Experimental setup for measuring the temperature change of the G & GC samples.

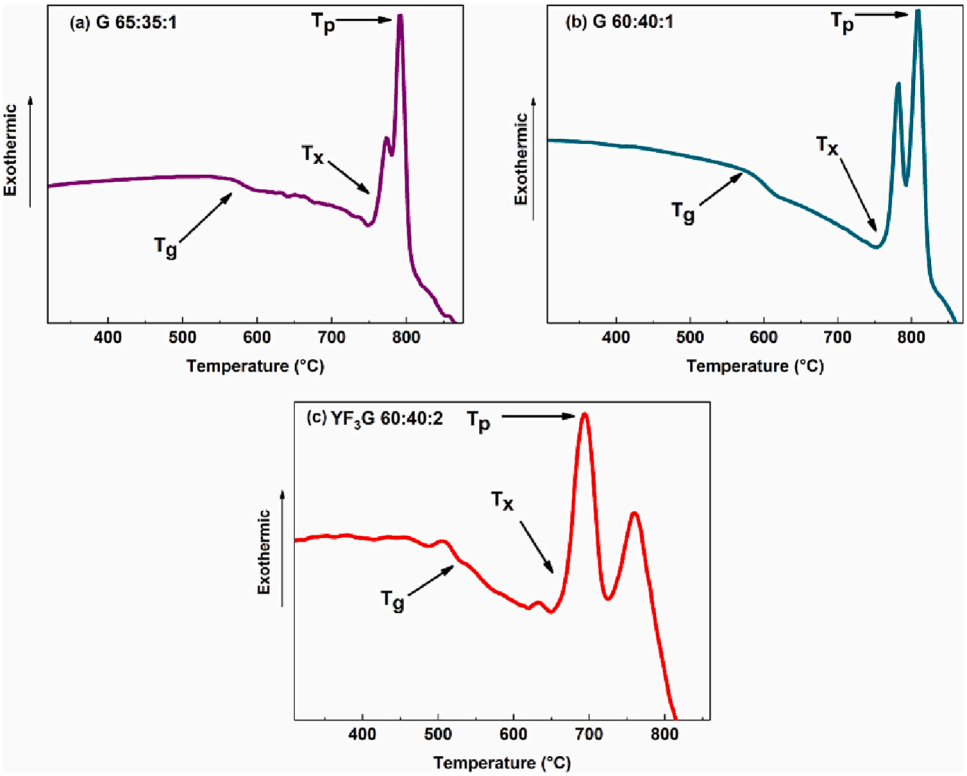


Fig. 2. DSC curve of the (a) G 65:35:1, (b) G 60:40:1 and (c) YF_3 G 60:40:2.

respectively. For GC 60:40:2, the transparency was ~78% and ~ 84% in the visible and NIR region respectively. But the parent glass (G 60:40:2) had a higher transparency of ~84% and ~ 95% in the visible and NIR region respectively (Fig. 3(b)). Owing to Rayleigh scattering caused by density changes in the glass by the presence of nanocrystals, atomic absorption and reflection the transparency reduces in glass ceramics compared to glasses [42].

The transparency around 980 nm of glass samples decreases with increasing ytterbium content, due to absorption from the $^2F_{7/2} \rightarrow {}^2F_{5/2}$ transition of Yb^{3+} ions. The transmittance was more than ~82% in the visible region and as high as ~90% in the NIR region for GC 60: 40: 1 which is higher than that of GC 60:40:2 (Fig. 3(c)).

The transmittance of GCs containing $YLiF_4$ crystals has been compared with that of the YF_3 GCs. YF_3 GCs present a much higher crystalline fraction compared to $YLiF_4$ GCs [37]. Note that a high crystallinity could mean that a higher amount of Yb^{3+} ions could be encapsulated inside the nanocrystals. Also, the smaller crystal diameters allow a higher transparency as shown in Fig. 2(d). The higher transparency in these glasses is obtained by controlling the crystal size to the nanometer scale. The XRD of the GCs with $YLiF_4$ and YF_3 are provided in Supplementary Information (SI Fig. 1). After 7 h of heat treatment at Tg + 60 °C, $YLiF_4$ containing GCs present crystals with mean diameters of 45 to 60 nm, estimated from Scherrer equation, but for YF_3GCs it was 26 to 31 nm. Also, to control the nucleation and growth processes of nanocrystals inside the glass matrix a detailed investigation on the crystallization mechanism was done through Ref 33. It was mentioned that the crystallization behavior difference between the two glasses is caused by a mixed effect of the viscosity and the ionic mobility during ceramization treatment.

One of the important parameters to take into consideration while designing glass based optical devices is the refractive index (RI). To understand the effect of oxide: fluoride ratio and ytterbium concentration on the refractive index (RI), we have investigated the RI through m-lines spectroscopy. The RI of the glasses and glass-ceramics at different wavelengths are shown in Fig. 4(a) and (b). As we decrease the oxide: fluoride (O/F) ratio, the refractive index increases, as expected. The introduction of polarizable fluorides enhances the refractive index and molar refractivity of the material [43]. Within the experimental uncertainty, the measured RI in transverse electric (TE) and transverse magnetic (TM) polarisation modes are equal. As a result, birefringence is negligible for GCs.

The refractive index decreases with increasing wavelength as expected [27]. Previous studies on $YLiF_4$ embedded transparent oxyfluoride glass–ceramics showed that the refractive index of the parent glasses at 632 nm were slightly lower compared with the GCs heat-treated at 550°C [26] and our results are in good agreement with that. The refractive index of YF_3GC 60:40:2 reduced due to the increasing content of fluorine. Fluorine has lower polarizability than that of oxygen (F = 0.557 $Å^3$, O = 0.802 $Å^3$). This property is used to reduce the refractive index of silica in the glass chemical vapor deposition process [44,45]. A similar trend can be observed here, both from base composition when comparing samples 65:35 and 60:40, and from final composition, with GC 60:40:2 and YF_3GC 60:40:2; the later having higher fluorine content.

According to R. I Epstein and M. Sheik Bahae the refractive index affects the optical cooling material in two different counteracting ways [46]. Firstly, it controls the escape of fluorescence light and secondly the rate for excited state spontaneous relaxation scales linearly with the local field correction factor which is given by the eq. (1).

$$\chi = \frac{n(n^2+2)^2}{9} \tag{1}$$

where n is the refractive index at the emission wavelength. They mentioned that the local field correction varies by a factor of three for typical laser cooled materials. In principle, higher radiative rates in higher RI materials can improve quantum yield and therefore the cooling efficiency. The local field correction factors are ~3.42, ~3.47, ~3.42 and 3.46 for GC 65:35:1, GC 60:40:1, GC 65:35:2 and GC 60:40:2 respectively. For YF_3GC 60:40:2 and the corresponding parent glass it

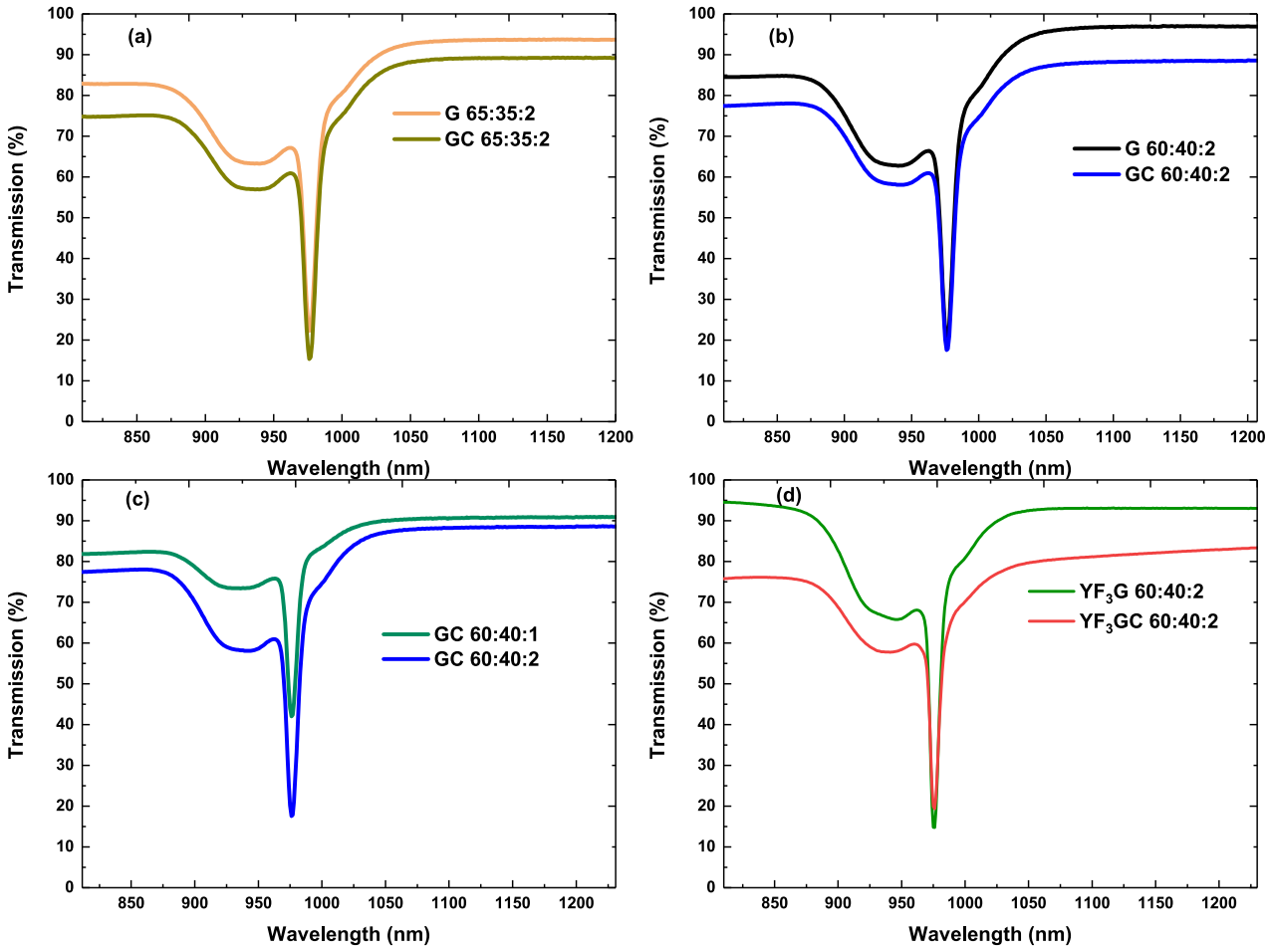


Fig. 3. The transmission spectra of (a) G 65:35:2 & GC 65:35:2, (b) G 60:40:2 & GC 60:40:2, (c) GC 60:40:1 & GC 60:40:2 and (d) YF_3G 60:40:2 & YF_3GC 60:40:2.

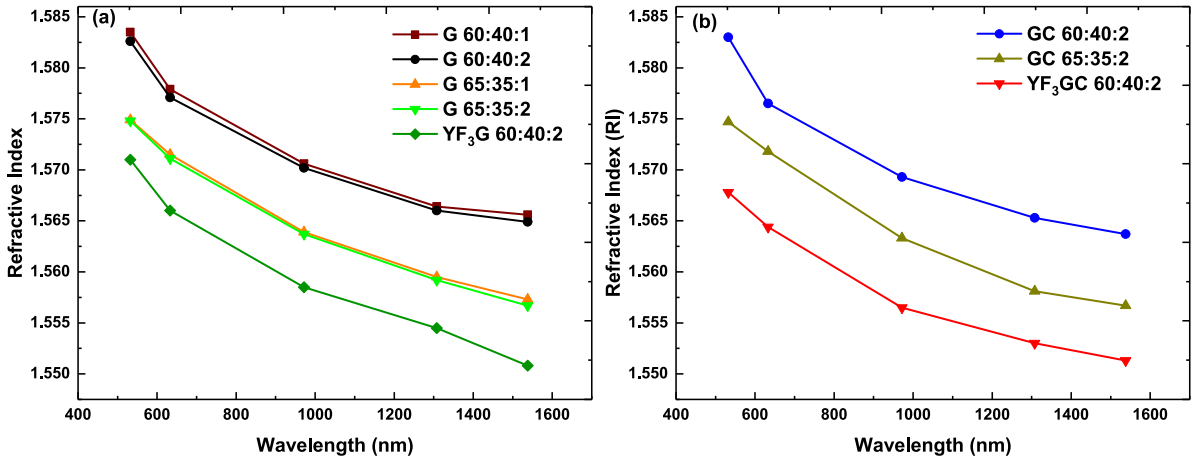


Fig. 4. The Refractive index values at 532.0, 632.8, 972.0, 1308.0 and 1538.0 nm for (a) all glass samples and (b) for GC 60:40:2, GC 65:35:2 and YF_3GC 60:40:2.

was ~3.37 and ~ 3.39 respectively. Even though the total internal reflection is high at higher RI, the advantage of high local field correction factors can counter the inconvenience caused by enhanced reabsorption. Therefore, tailoring the local field correction factor of the laser cooling material is of great importance. Our findings in Fig. 4 (a & b) highlight the fact that, using oxyfluoride glass ceramics, the RI and the local field correction factor can be adjusted by simply changing the volume fractions of the glass constituents, for example by adding or reducing the content of fluorides.

3.3. Photoluminescence (PL) properties

Consider the ground and excited electronic states in the oxyfluoride glass doped with Yb ions, both of which are split into several sub-levels by the crystal field. We excite the system with energy $E_p = hc/\lambda_p$. In a picosecond time scale, electron-phonon interaction will establish a Boltzmann equilibrium population in the excited state manifold. The mean fluorescence energy, $E_f = hc/\lambda_f$ depends on the temperature and

the crystal-field splitting of the glass. When we excite the system at $Ep < E_f$, an energy difference of $\Delta E = E_f - E_p$ is required to establish thermal equilibrium and that will be provided by the phonons in the solid. The excited electrons decay by radiative relaxation which leads to cooling of the system. The PL characteristics of RE ions in inorganic glasses are determined by host material composition, the concentration of RE ions, and the pump power [47]. Along with these factors, the total phonon energy of the material mainly influences the PL emission efficiency of excited states of Yb^{3+} ions in the investigated glasses. We studied the spectroscopic properties of all the investigated glasses and GCs in detail to assess the cooling potentiality of these materials.

In Yb-doped glasses, the PL emission spectra possess the same shape despite the excitation wavelength, as a result of the thermal re-equilibrium processes (~ns) is significantly faster than the radiative lifetime (~ms) [47]. Fig. 5(a) and (b) shows the obtained room temperature PL spectra of glasses and glass ceramic doped with 1 mol% and 2 mol%, respectively at an excitation wavelength of 980 nm. In GC 65:35:1 and GC 60:40:1, the PL emission observed around 1010 nm indicates that Yb^{3+} ions were incorporated into the fluoride phase. As we increased the Yb content from 1 to 2 mol% the mean fluorescence wavelength (MFW) changed from 1010 nm to 1013 nm. The PL intensity in GCs is higher compared to the parent glasses. This indicates that the formation of crystallites altered the environment of the Yb^{3+} ions, resulting from ion migration either into the $YLiF_4$ crystals or towards the nanocrystal/glass boundary. The probability of multi-phonon relaxations reduces in GCs with low phonon energies and therefore the intensity of the PL emission increases. According to the Miyakawa and Dexter theory [48], the multi-phonon decay rate relies exponentially on the energy gap difference between the energy levels and the phonon energy of the material. Silicate oxide glass possesses a maximum phonon energy of 1100 cm^{-1}, but it reduces to 250 cm^{-1} for a $YLiF_4$ crystal. Moreover, it should be mentioned the PL intensity scales with fluoride content (~40%). Since Yb^{3+} ions possess large absorption cross section at 980 nm, the emission intensity is approximately 7 times larger than that recorded under 1020 nm excitation. To further investigate and assess the role of crystallinity in the PL emission enhancement of glass ceramic, we compared GCs containing YF_3 crystals (YF_3GC 60:40:2) and $YLiF_4$ crystals (GC 60:40:2) while exciting with 980 and 1020 nm. Due to the higher crystalline fraction, YF_3GC 60:40:2 has a higher PL intensity centred at 1016 nm (Fig. 6(a) & (b)) at a pump wavelength of 980 or 1020 nm than that of GC 60:40:2.

To probe the effect of compositional variations on the internal quantum yield (iQY) of all the samples at several excitation wavelengths, we used an integrating sphere method [23,25,26] which is shown in Table 2. The iQY values of GCs were larger than that of Gs as expected. For the GC 65:35:2, the iQY varies between 68% and 94% for different excitation wavelengths. For GC 60:40:2 the iQY values at different excitation wavelengths varies between 71% and 95%. Samples with 2 mol% of Yb possess higher iQY values at pump wavelengths of 1000 and 1020 nm. The PL intensity as well as iQY in GCs were larger than that of parent glasses and provided the advantage of low phonon energy crystals. The external quantum yield (eQY) of all samples was less than 15% due to radiation trapping effects [23].

The quantum efficiency of the GC 60:40:2 sample at an excitation of 1020 nm was obtained as 71% and it was elevated to 76% with the increase in the crystallinity in YF_3GC 60:40:2 samples. Along with the results obtained in this study for Yb doped GC 60:40:2 and YF_3GC 60:40:2, it should be noted that through a suitable compositional modification and purification process an enhancement in quantum yield could be expected as mentioned in Section 3.5.

It has been observed in all the investigated glass and glass ceramic samples that the PL emission decay from the $4F_{5/2}$ level follow a single exponential time dependence. Table 3 provides the PL emission decay time values of Yb^{3+}: $2F_{5/2}$ level at a pump wavelength of 920 nm obtained by fitting the decay curves using a single exponential function.

Gs and GCs containing larger amounts of fluoride content with 2 mol % of Yb demonstrate a longer lifetime. Compared with the parent glasses, the GC samples exhibited longer lifetimes. The majority of Yb^{3+} ions are placed inside the $YLiF_4$ nanocrystals that are precipitated in the glass during the thermal treatment. Consequently, the multi-phonon decay rate in the Yb^{3+} ions inside the $YLiF_4$ crystals is reduced and therefore, the lifetime of the ions inside the nanocrystals is longer. In GC 65:35:1 and GC 65:35:2 the fluorine content was reduced and as a result the lifetime of the Yb^{3+} ions are reduced compared to the GC 60:40:1 and GC 60:40:2 due to the higher phonon energy of the glass. The addition of fluoride promotes the experimental lifetime increase, as previously reported in Yb^{3+}doped tellurite glasses [49].

The luminescence lifetime (τ) values ascribed to the Yb^{3+}: $^2F_{5/2}$ level for YF_3GC 60:40:2 under excitation at 920 nm is also provided in Table 3. The decay curves are given in Supplementary Information (SI Fig. 2). We observe that the YF_3GC 60:40:2 has a slightly longer lifetime than the GC 60:40:2 as it contains more fluoride and has more ytterbium inside the nanocrystals. Also, as previously stated, YF_3 GCs are more crystalline than $YLiF_4$ GCs, so the averaged lifetime of Yb^{3+} in YF_3GC 60:40:2 is much longer than that in GC 60:40:2.

Radiation trapping can occur in the glass due to total internal

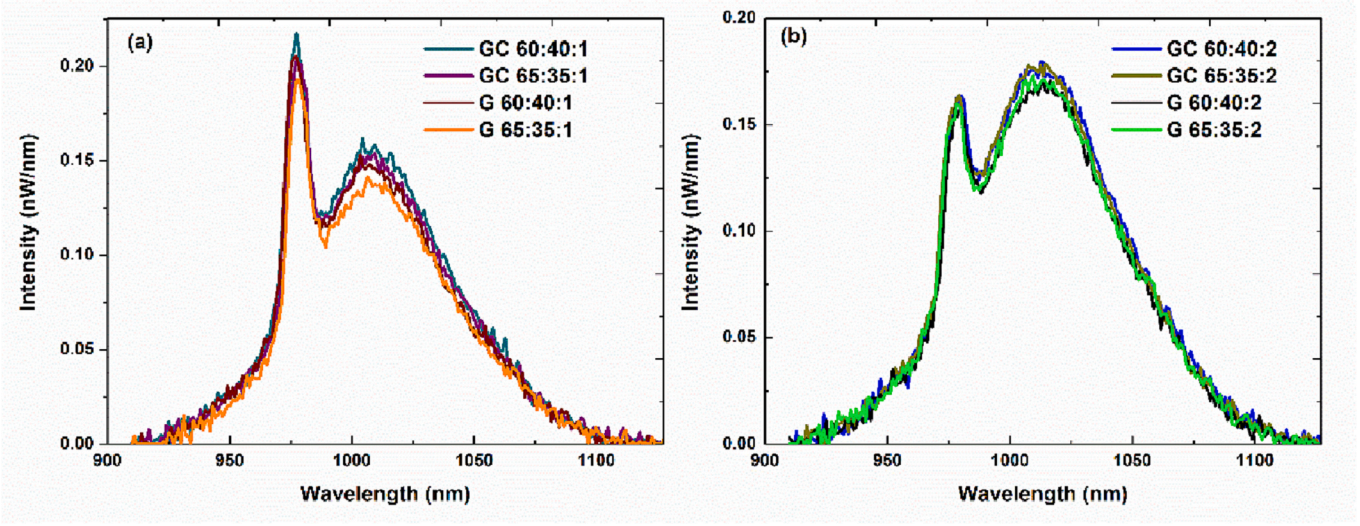


Fig. 5. (a) The PL emission spectra of GCs & corresponding parent glasses doped with 1 mol% Yb using a pump wavelength of 980 nm and (b) The PL emission spectra of glass ceramics & corresponding parent glasses doped with 2 mol% Yb at a pump wavelength of 980 nm.

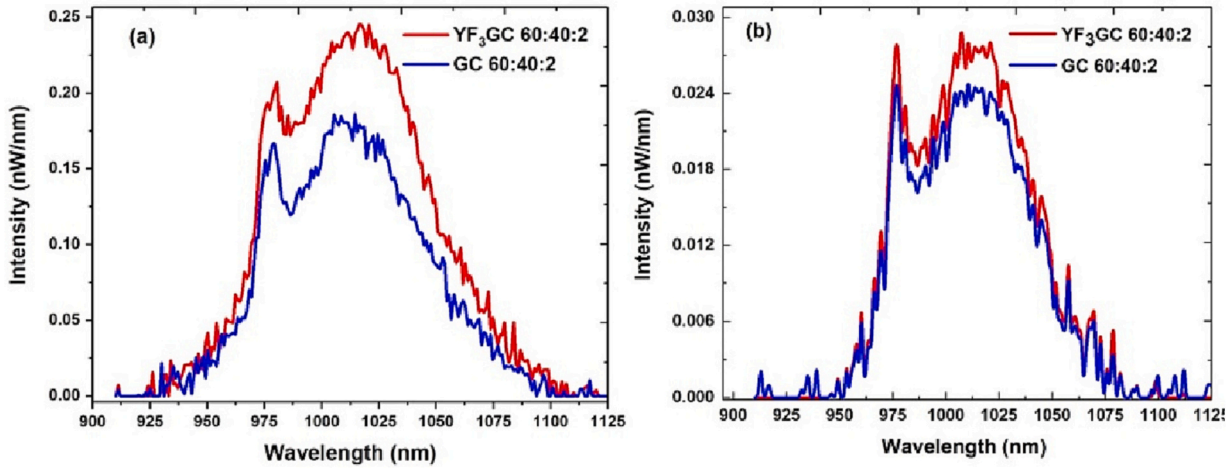


Fig. 6. (a) The PL emission spectra of YF_3GC 60:40:2 & GC 60:40:2 with the corresponding parent glasses with a pump wavelength of (a) 980 nm, (b) Comparison of the PL emission spectra of YF_3GC 60:40:2 & GC 60:40:2 with a pump wavelength of 1020 nm.

Table 2
The measured internal quantum yield (iQY) of all the glasses and glass ceramics using different pump wavelengths.

	Internal quantum yield (iQY) (in %)		
Glass Composition	920 nm	980 nm	1000 nm
G 65:35:1	67	58	55
G 60:40:1	57	66	49
G 65:35:2	52	77	67
G 60:40:2	65	79	70
YF_3G 60:40:2	67	83	74

	Internal Quantum yield (iQY) (in %)			
Glass-ceramic Composition	920 nm	980 nm	1000 nm	1020 nm
GC 65:35:1	70	98	75	64
GC 60:40:1	77	99	75	65
GC 65:35:2	72	94	76	68
GC 60:40:2	80	95	79	71
YF_3GC 60:40:2	84	96	80	76

Table 3
PL emission decay time values of Yb^{3+}: $^2F_{5/2}$ level in all glasses and glass-ceramics.

Sample	Lifetime (ms)	Sample	Lifetime (ms)
G 65:35:1	1.37	GC 65:35:1	1.37
G 60:40:1	1.37	GC 60:40:1	1.41
G 65:35:2	1.38	GC 65:35:2	1.38
G 60:40:2	1.41	GC 60:40:2	1.44
YF_3G 60:40:2	1.51	YF_3GC 60:40:2	1.55

reflection and can lead to reduction in cooling efficiency due to re-absorption. This relies on the RI difference of the cooling medium from the surrounding media.

The fluorescence extraction efficiency is given by the eq. (2) [50].

$$\eta_e = 3\left(1 - \left(1 - \left(\frac{1}{n}\right)^{2^{1/2}}\right) exp(-\alpha_r(\lambda) l\,)\right) \quad (2)$$

where n is the RI of the cooling medium, α_r is the resonant absorption coefficient, and l is the length of the medium. The fluorescence reabsorption along the length l of a sample is considered using the exponential factor. The extraction efficiency of all glass ceramics at a wavelength of 1030 nm is given in Table 4. The YF_3GC 60:40:2 has a higher extraction efficiency of 69.0% compared to other samples under investigation.

Table 4
The extraction efficiency of all glass ceramics at a wavelength of 1030 nm.

GC composition	GC 65:35:1	GC 60:40:1	GC 65:35:2	GC 60:40:2	YF_3GC 60:40:2
Extraction efficiency (η_e)	67.6%	67.4%	65.7%	63.4%	69.0%

3.4. Calorimetry

The presence of anti-Stokes emission along with higher quantum efficiency in all glass ceramics motivated us to perform additional investigations on the potentiality of this material as a cooling media.

The steady state glass-ceramic temperature (ΔT) was extracted using the FBG direct contact method [38] and P_{abs} is calculated from the input and transmitted laser powers along with the known absorption spectra of the glasses. To elucidate the temperature change at different pump wavelengths ranging from 980 to 1040 nm, we plotted the temperature changes (ΔT in Kelvin) normalized by the absorbed laser pump power (in Watt) supplied to the samples (Fig. 7(a) and (b)). Beginning at 980 nm, significant heating ($\Delta T/ P_{Abs} \sim$ 15–22 K/W) is observed in all samples. But the temperature was significantly reduced near a pump wavelength of ~1030 nm (0.6–3.0 K/W). Beyond 1030 nm the samples heat due to the background absorption. The GC sample with higher fluoride content and lower oxide content having 2 mol% of ytterbium demonstrates the lowest heating compared to the other samples.

We then compared the cooling potentiality of GCs containing YF_3 nano crystals and glass ceramics containing $YLiF_4$ crystals. The temperature dynamics of YF_3GC 60:40:2 at various pump wavelengths varying from 1000 to 1032 nm is shown in Fig. 8. For YF_3GC 60:40:2, the maximum $\Delta T /P_{Abs}$ was of ~0.4 K/W at a pump wavelength of 1032 nm. This is the most striking finding of this study, namely, that the highly crystalline YF_3 GCs exhibit higher quantum efficiency and greater temperature reduction than that of lower crystallinity $YLiF_4$ glass ceramic obtained from the same initial composition. The change in optimum pump wavelength for both types of glasses can be ascribed to the change in MFW as well as the change in the resonant absorption coefficient.

However, the higher background absorption in these glasses preclude the possibility of observation of laser induced cooling. More insight would be extracted from the background absorption coefficient

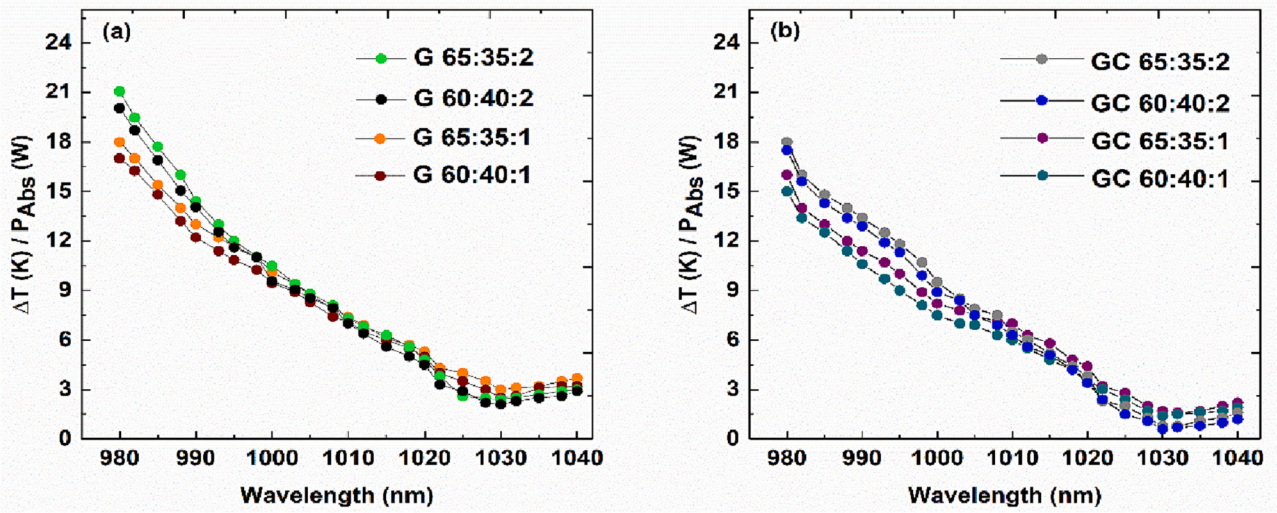


Fig. 7. (a) The temperature variations of all Gs normalized by absorbed power ($\Delta T / P_{Abs}$) for different pump wavelengths varying from 980 nm to 1040 nm, (b) The temperature variations of all GCs normalized by absorbed power ($\Delta T / P_{Abs}$) for different pump wavelengths varying from 980 nm to 1040 nm.

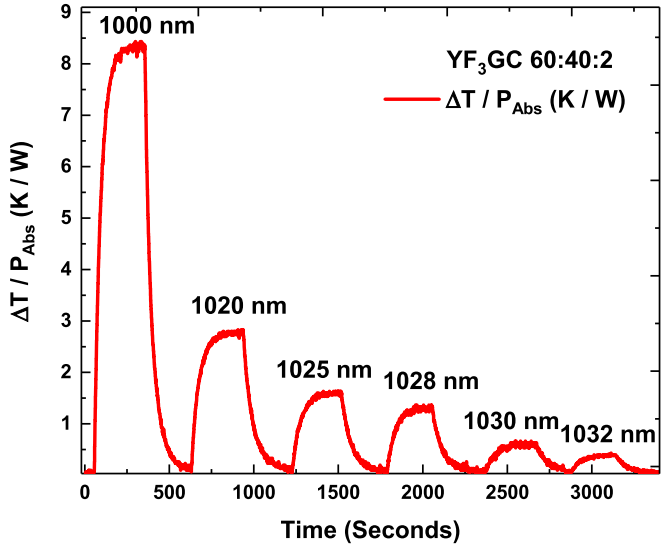


Fig. 8. The temperature change as a function of time for the YF_3GC 60:40:2 at different pump wavelengths varying from 1000 to 1032 nm.

since it is one of the generally used procedures to know the impurity level in laser cooling materials. The background absorption coefficient (α_b) determined using calorimetric technique [51] is provided in Table 5. The α_b lies in the range of 0.14–0.15 m^{-1} in all the GCs we investigated, which is not low enough to cool.

To examine the cause of background absorption, we conducted elemental analysis using ICP measurements. It was determined that the main impurity that needed to be reduced in order to improve cooling performance was Fe^{3+}. The amount of Fe was estimated to be ~21 ppm. For achieving cooling, the highest value of quantum yield and the lowest one for background absorption is required. For improving the performance of these glass ceramics, minimization of impurities in the glass host is necessary which can be achieved by sample preparation in controlled environments and by the use of high purity precursors. Once this problem is entirely resolved, we will be able to control the optical behavior of these glass ceramics and therefore tackle the practical optical cooling issues.

Table 5
The background absorption coefficient of all the investigated glass ceramics.

Sample	Background absorption coefficient (α_b)
GC 65:35:1	0.154 m^{-1}
GC 60:40:1	0.148 m^{-1}
GC 65:35:2	0.159 m^{-1}
GC 60:40:2	0.157 m^{-1}
YF_3GC 60:40:2	0.152 m^{-1}

3.5. *Effect of purification on the optical properties of glasses*

Although the role of impurities is not clear in the present study, the PL quantum yield is expected to be significantly enhanced after purification, which is a crucial subject for a future study. It is worthwhile to highlight that our first step of the purification of precursor materials used to synthesize GCs containing $YLiF_4$ crystals via chelated assisted extraction (CASE) purification method [35] improved the PL emission intensity and quantum yield. The precursor materials were purified using APDC-MIBK chelate cleaning process followed by re-fluorination using high purity HF [52]. The chelate agent was employed to bind to impurities/metal ions in an aqueous phase before transferring the metal-chelate complexes to a second organic phase [35,52]. We noticed a reduction in the α_b to 0.095 m^{-1} from 0.157 m^{-1} after the purification.

Figure 9 shows the PL emission spectra of purified GC and normal GC (GC 60:40:2) at a pump wavelength of 980 nm. The quantum efficiency of the GC 60:40:2 sample at an excitation of 980 nm was obtained as 95% and it was elevated to 98% after purification. Also, in contrast to prior experiments, the CASE purification helped in obtaining the best quantum yield of 78%, with a pump wavelength of 1020 nm. The higher iQY value of purified GC indicates that through purification the non-radiative contribution of the glass was reduced and therefore the luminescent efficiency was increased. This purification non-optimized process only led to a reduction of iron concentration to 8 ppm which is good but not enough to cool the material.

The lifetime (τ) of GC 60:40:2 was evaluated before and after purification to investigate the effect of purification in influencing the PL characteristics. The τ value for the G and GC increased 1.60 and 1.62 ms from 1.41 and 1.44 ms, respectively after purification. This is compelling evidence of reduction in the non-radiative contributions of impurities and we'd like to exploit this in a future study to obtain maximum temperature reduction. Further study of background absorption and elemental analysis is desired in each step of purification because the small amount of impurities even with few ppm can preclude the observation of real cooling [53]. Improved sample quality and precursor

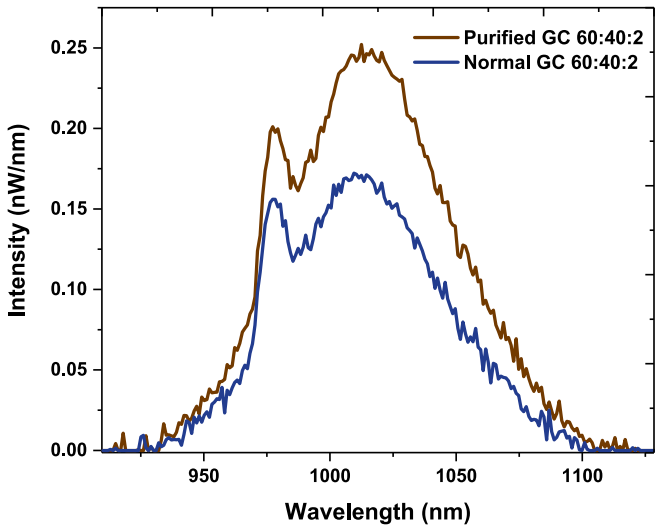


Fig. 9. The PL emission spectra of purified GC 60:40:2 and normal GC 60:40:2 (without purification) with a pump wavelength of 980 nm.

purification can help to tackle these while also providing more direct proof of optical cooling.

The effect of CASE purification on the structural and spectroscopic properties of these GCs are the subject of another article in preparation. However, the present result opens the possibility of optical cooling in glass ceramics, which are significant roadblocks for important applications, such as sensors, heat balanced laser systems and satellite instrumentations. Our findings also give a starting point for further research into the compositional diversity in these glass ceramics for optical cooling applications.

4. Conclusions

In conclusion, the optical properties of ytterbium doped highly transparent glass–ceramics containing $YLiF_4$ or YF_3 nanocrystals were studied exploring the effect of compositional variations (O/F ratio and crystallinity) and ytterbium content for laser cooling applications. The glass-ceramics and corresponding parent glasses were systematically analyzed for thermal and optical properties through DSC, absorption and fluorescence spectral measurements. Our work evidence that the optimization of oxide: fluoride ratio and rare earth ion concentration in these glass ceramics are necessary to obtain high photoluminescent quantum yield. Samples having higher fluoride content with 2 mol% of Yb possess higher iQY value of 71% at 1020 nm, which is beneficial for laser cooling. This was elevated to 76% with the increase in crystallinity as well as fluorine concentration in YF_3GC samples. The enhanced lifetime and quantum yield performance is expected to facilitate the application of oxyfluoride glass ceramics in laser cooling applications.

Calorimetric measurements performed on these glasses showed that the GC sample containing $YLiF_4$ nano crystals with higher fluoride content and lower oxide content having 2 mol% of ytterbium presented fewer heating effects compared to the others. Highly crystalline YF_3GCs exhibit higher quantum efficiency and larger temperature reduction than that of lower crystalline $YLiF_4$ glass ceramic obtained from the same initial composition.

The main obstacle to simultaneously achieving high quantum efficiency and low background absorption for glass ceramics must be overcome before they could possibly be a viable material for laser cooling applications. The enhanced PL emission, lifetime and higher internal quantum yield value of 78% achieved using purified GC at 1020 nm indicates that the purification helps to decrease the non-radiative contribution in the glass and consequently enhances the luminescent efficiency. Our findings offer a unique insight into exploring the compositional variations in the ytterbium doped oxyfluoride glass ceramics as a promising candidate for laser cooling.

Declaration of Competing Interest

The authors declare that they have no known competing financial interests or personal relationships that could have appeared to influence the work reported in this paper.

Data availability

Data will be made available on request.

Acknowledgements

The authors acknowledge the Natural Sciences and Engineering Research Council of Canada (NSERC), Canadian Excellence Research Chair program (CERC) on Photonic Innovations, Fonds Québecois de la Recherche sur la Nature et les Technologies (FQRNT), Merit scholarship program for foreign students (PBEEE Quebec-India) and Canada Foundation for Innovation (CFI).

Appendix A. Supplementary data

Supplementary data to this article can be found online at https://doi.org/10.1016/j.nocx.2023.100173.

References

[1] M.P. Hehlen, J. Meng, A.R. Albrecht, E.R. Lee, A. Gragossian, S.P. Love, C. E. Hamilton, R.I. Epstein, M. Sheik-Bahae, First demonstration of an all-solid-state optical cryocooler, Light Sci. Appl. 7 (2018) 15.
[2] G.L. Mills, A.J. Mord, P.A. Slaymaker, Design and predicted performance of an optical cryocooler for a focal plane application, in: R.G. Ross (Ed.), Cryocoolers 11, Springer, Boston, MA, 2002.
[3] P. Pringsheim, Zwei bemerkungen uber den unterschied von lumineszenz-und temperaturstrahlung, Z. Phys. 57 (11–12) (1929) 739–746.
[4] R.I. Epstein, M.I. Buchwald, B.C. Edwards, T.R. Gosnell, C.E. Mungan, Observation of laser-induced fluorescent cooling of a solid, Nature 377 (1995) 500–503.
[5] D.V. Seletskiy, S.D. Melgaard, S. Bigotta, A. Di Lieto, M. Tonelli, M. Sheik-Bahae, Laser cooling of solids to cryogenic temperatures, Nat. Photonics 4 (3) (2010) 161–164.
[6] T. Kushida, J.E. Geusic, Optical refrigeration in Nd-doped yttrium aluminum garnet, Phys. Rev. Lett. 21 (16) (1968) 1172–1175.
[7] S.R. Bowman, C.E. Mungan, New materials for optical cooling, Appl. Phys. B Lasers Opt. 71 (2000) 807–811.
[8] G. Nemova, R. Kashyap, Laser cooling with PbSe colloidal quantum dots, J. Opt. Soc. Am. B 29 (2012) 676–682.
[9] E. Mobini, S. Rostami, M. Peysokhan, A. Albrecht, S. Kuhn, S. Hein, C. Hupel, J. Nold, N. Haarlammert, T. Schreiber, R. Eberhardt, A. Tunnermann, M. Sheik-bahae, A. Mafi, Laser cooling of ytterbium-doped silica glass, Commun. Phys. 3 (2020) 134.
[10] T.R. Gosnell, Laser Cooling by 65 K of Yb^{3+}-Doped ZBLANP Glass, in Quantum Electronics and Laser Science Conference, in: T. Gallagher, H. Van Driel, H. Gibbs, D. Wineland (Eds.), OSA Technical Digest, Optical Society of America, 2000 paper QThF2.
[11] C.W. Hoyt, M.P. Hasselbeck, M. Sheik-Bahae, R.I. Epstein, S. Greenfield, J. Thiede, J. Distel, J. Valencia, Advances in laser cooling of thulium-doped glass, J. Opt. Soc. Am. B 20 (2003) 1066–1074.
[12] E. Mobini, S. Rostami, M. Peysokhan, A. Albrecht, S. Kuhn, S. Hein, C. Hupel, J. Nold, N. Haarlammert, T. Schreiber, R. Eberhardt, Laser cooling of ytterbium-doped silica glass, Commun. Phys. 3 (2020) 134.
[13] Y. Wang, J. Ohwaki, New transparent vitro-ceramics co-doped with Er^{3+} and Yb^{3+} for efficient frequency up conversion, Appl. Phys. Lett. 63 (1993) 3268–3270.
[14] B. Aktas, M. Albaskar, S. Yalcin, K. Dogru, Optical properties of soda-lime-silica glasses doped with peanut shell powder, Arch. Mater. Sci. Eng. 82 (2) (2016) 57–61.
[15] B. Aktas, M. Albaskara, S. Yalcin, K. Dogru, Optical properties of soda-lime-silica glasses doped with eggshell powder, Acta Phys. Pol. A 132 (3) (2017) 442–444.
[16] A. Acikgoz, G. Ceyhan, B. Aktas, S. Yalcin, G. Demircan, Luminescent, structural and mechanical properties of erbium oxide doped natural obsidian glasses, J. Non-Cryst. Solids 572 (2021), 121104.
[17] Effect of Er_2O_3 on structural, mechanical, and optical properties of Al_2O_3-Na_2O-B_2O_3-SiO_2 glass, J. Non-Cryst. Solids 584 (2022), 121516.
[18] Y. Kawamoto, R. Kanno, J. Qiu, Up-conversion luminescence of Er^{3+} in transparent SiO_2—PbF_2—ErF_3 glass ceramics, J. Mater. Sci. 33 (1998) 63–67.

[19] A. Pablos-Martín, N. Hémono, G.C. Mathe, S. Bhattacharyya, T. Höche, H. Bornhöft, J. Deubener, F. Muñoz, A. Durán, M.J. Pascual, Crystallization kinetics of LaF_3 nanocrystals in an oxyfluoride glass, J. Am. Ceram. Soc. 94 (2011) 2420–2428.
[20] K. Biswas, A.D. Sontakke, J. Ghosh, K. Annapurna, Enhanced blue emission from transparent oxyfluoride glass–ceramics containing Pr^{3+}: BaF_2 nanocrystals, J. Am. Ceram. Soc. 93 (2010) 1010–1017.
[21] F. Liu, Y. Wang, D. Chen, Y. Yu, E. Ma, L. Zhou, P. Huang, Up conversion emission of a novel glass ceramic containing Er^{3+}: $BaYF_5$ nanocrystals, Mater. Lett. 61 (2007) 5022–5025.
[22] F. Liu, E. Ma, D. Chen, Y. Yu, Y. Wang, Tunable red-green up conversion luminescence in novel transparent glass ceramics containing Er: $NaYF_4$ nanocrystals, J. Phys. Chem. B 110 (42) (2006) 20843–20846.
[23] J. Thomas, L.J.Q. Maia, Y. Ledemi, Y. Messaddeq, R. Kashyap, Emerging trends, challenges, and applications in solid-state laser cooling, in: A. Ray (Ed.), Oxide Electronics, 2021, pp. 353–396.
[24] G. Nemova, R. Kashyap, Laser cooling with Tm^{3+} −doped oxy-fluoride glass ceramic, J. Opt. Soc. Am. B 29 (2012) 3034–3038.
[25] E. Soares de Lima Filho, K.V. Krishnaiah, Y. Ledemi, Y. Yu, Y. Messaddeq, G. Nemova, R. Kashyap, Ytterbium-doped glass-ceramics for optical refrigeration, Opt. Express 23 (2015) 4630–4640.
[26] K.V. Krishnaiah, E. Soares de Lima Filho, Y. Ledemi, G. Nemova, Y. Messaddeq, R. Kashyap, Development of ytterbium-doped oxyfluoride glasses for laser cooling applications, Sci. Rep. 6 (2016) 21905.
[27] K.V. Krishnaiah, Y. Ledemi, E. Soares de Lima Filho, G. Nemova, Y. Messaddeq, R. Kashyap, Development of Yb^{3+}-doped oxyfluoride glass-ceramics with low OH− content containing CaF_2 nanocrystals for optical refrigeration, Opt. Eng. 56 (1) (2016), 011103.
[28] L.J.Q. Maia, J. Thomas, K.V. Krishnaiah, Y. Ledemi, D. Seletskiy, Y. Messaddeq, R. Kashyap, Structural and optical characterizations of Yb^{3+} doped GeO_2-PbF_2-PbO glass-ceramics for optical refrigeration, in: Proc. SPIE., Optical and Electronic Cooling of Solids III, 2018, 105500O.
[29] L.J.Q. Maia, J. Thomas, Y. Ledemi, K.V. Krishnaiah, D. Seletskiy, Y. Messaddeq, R. Kashyap, Photonic properties of novel Yb^{3+} doped germanium-lead oxyfluoride glass-ceramics for laser cooling applications, Front. Optoelectron. 11 (2018) 189–198.
[30] J. Thomas, T. Meyneng, Y. Ledemi, A. Rakotonandrasana, D. Seletskiy, L.J.Q. Maia, Y. Messaddeq, R. Kashyap, Oxyfluoride glass-ceramics: a bright future for laser cooling, in: Proc. SPIE 11298, Photonic Heat Engines: Science and Applications II, 112980E, 2020.
[31] T. Suzuki, S. Masaki, K. Mizuno, Y. Ohishi, Preparation of novel transparent glass–ceramics containing fluoride crystals, Opt. Mater. 33 (2011) 12.
[32] D. Deng, S. Xu, S. Zhao, C. Li, H. Wang, H. Ju, Enhancement of up-conversion luminescence in $Tm^{3+}/Er^{3+}/Yb^{3+}$-codoped glass ceramic containing $LiYF_4$ nanocrystals, J. Lumin. 129 (11) (2009) 1266–1270.
[33] D. Deng, S. Xu, R. Bao, S. Zhao, B. Wang, H. Wang, H. Ju, Blue cooperative upconversion in Yb^{3+}-doped glass ceramic containing $LiYF_4$ nanocrystals, J. Phys. D. Appl. Phys. 42 (2009), 105111.
[34] F. Okada, S. Togawa, K. Ohta, Solid-state ultraviolet tunable laser: A Ce^{3+} doped $LiYF_4$ crystal, J. Appl. Phys. 75 (l) (1994) 49–53.
[35] W.M. Patterson, P.C. Stark, T.M. Yoshida, M. Sheik-Bahae, M.P. Hehlen, Preparation and characterization of high-purity metal fluorides for photonic applications, J. Am. Ceram. Soc. 94 (9) (2011) 2896–2901.
[36] M.P. Hehlen, W.L. Boncher, S.D. Melgaard, M.W. Blair, R.A. Jackson, T. E. Littleford, S.P. Love, Preparation of high purity LiF, YF_3, and YbF_3 for laser refrigeration, in: Proc. SPIE 9000, Laser Refrigeration of Solids VII, 2014, 900004.
[37] T. Meyneng, J. Thomas, Y. Ledemi, M. Allix, E. Veron, C. Genevois, R. Kashyap, Y. Messaddeq, The role of fluorine in high quantum yield oxyfluoride glasses and glass-ceramics, J. Alloys Compd. 900 (2022), 163512.
[38] E. Soares de Lima Filho, M.D. Baiad, M. Gagné, R. Kashyap, Fiber Bragg gratings for low-temperature measurement, Opt. Express 22 (2014) 27681–27694.
[39] P.P. Fedorov, A.A. Luginina, A.I. Popov, Transparent oxyfluoride glass ceramics, J. Fluor. Chem. 172 (2015) 22–50.
[40] A.R. Marquesi, J.R.J. Delbeni, A.A.S.T. Delben, Glass forming ability and thermal stability of oxyfluoride glasses, J. Therm. Anal. Calorim. 96 (2) (2009) 403–406.
[41] M. Sroda, Effect of LaF_3 admixture on thermal stability of borosilicate glasses, J. Therm. Anal. Calorim. 88 (2007) 245–249.
[42] S. Hendy, Light scattering in transparent glass ceramics, Appl. Phys. Lett. 81 (2002) 1171–1173.
[43] D.R. MacFarlane, P.J. Newman, Z. Zhou, J. Javorniczky, Systematic study of refractive index variations with composition in heavy metal fluoride glasses, J. Non-Cryst. Solids 161 (1993) 182–187.
[44] H. Wehr, D. Wiechert, Refractive index and density of fluorine doped silica prepared by the PCVD process, Mater. Res. Bull. 21 (5) (1986) 559–566.
[45] J.W. Fleming, D.L. Wood, Refractive index dispersion and related properties in fluorine doped silica, Appl. Opt. 22 (19) (1983) 3102.
[46] R.I. Epstein, M. Sheik-bahae, Optical Refrigeration: Science and Applications of Laser Cooling of Solids, 2009.
[47] Michel J.F. Digonnet (Ed.), Optical and Electronic Properties of Rare Earth Ions in Glasses, in Rare-Earth-Doped Fiber Lasers and Amplifiers, Revised and Expanded, CRC Press, New York, 2001.
[48] T. Miyakawa, D.L. Dexter, Phonon sidebands, multi-phonon relaxation of excited states, and phonon-assisted energy transfer between ions in solids, Phys. Rev. B 1 (7) (1970) 2961–2969.
[49] G. Wang, S. Dai, J. Zhang, S. Xu, L. Hu, Z. Jiang, Effect of F^- ions on emission cross-section and fluorescence lifetime of Yb^{3+}-doped tellurite glasses, J. Non-Cryst. Solids 351 (24–26) (2005) 2147–2151.
[50] C.W. Hoyt, Laser Cooling in Thulium Doped Solids, Dissertation, University of New Mexico, 2003.
[51] E. Soares de Lima Filho, G. Nemova, S. Loranger, R. Kashyap, Laser-induced cooling of a Yb: YAG crystal in air at atmospheric pressure, Opt. Express 21 (2013) 24711–24720.
[52] J. Thomas, T. Meyneng, Y. Ledemi, D. Seletskiey, Y. Messaddeq, R. Kashyap, Impact of purification on the optical properties of oxyfluoride glass ceramics for laser cooling applications, in: Laser Congress 2021 (ASSL, LAC), Optica Publishing Group, 2021 paper JM3A.47.
[53] A. Di Lieto, A. Sottil, A. Volp, Z. Zhang, D.V. Seletskiy, M. Tonelli, Influence of other rare earth ions on the optical refrigeration efficiency in Yb: YLF crystals, Opt. Express 22 (2014) 28572–28583.